The dynamic range and domain-specific signals of intracellular calcium in photoreceptors

T. Szikra and D. Krizaj

Dept. of Ophthalmology, UCSF School of Medicine, San Francisco, CA 94143-0730

Section Editor Cellular Neuroscience

C. Sotelo, Ph.D.
INSERM U-106, Batiment de Pediatrie, Hopital de la Salpetriere,
47 Bd de l'Hopital, 75651 Paris Cedex 13, France

Corresponding author:

David Krizaj, Ph.D.
Dept. of Ophthalmology
UCSF School of Medicine
10 Koret Way, Rm K-131
Tel: (415) 502-3864
Fax: (415) 476-6289
E-mail: krizaj@phy.ucsf.edu

Abbreviations: $[Ca^{2+}]i$, intracellular calcium concentration; $InsP_3$, inositol triphosphate; OS, outer segment; PMCA, plasma membrane calcium ATPase; SERCA, sarcoplasmic-endoplasmic reticulum calcium ATPase; TMRM, tetramethylrhodamine.

Abstract

Vertebrate photoreceptors consist of strictly delimited subcellular domains - the outer segment, ellipsoid, cell body and synaptic terminal, each hosting crucial cellular functions, including phototransduction, oxidative metabolism, gene expression and transmitter release. We used optical imaging to explore the spatiotemporal dynamics of Ca^{2+} signaling in non-outer segment regions of rods and cones. Sustained depolarization, designed to emulate photoreceptor activation in the darkness, evoked a standing Ca^{2+} gradient with spatially-averaged $[Ca^{2+}]i$ within synaptic terminals of ~ 2 μM and lower (~900 nM) $[Ca^{2+}]i$ in the ellipsoid. Measurements from axotomized cell bodies and isolated ellipsoids showed that Ca^{2+} enters the two compartments via both local L-type Ca^{2+} channels and diffusion. The results from optical imaging studies were supported by immunostaining analysis. L-type voltage-operated Ca^{2+} channels and plasma membrane Ca^{2+} ATPases (PMCAs) were highly expressed in synaptic terminals with progressively lower expression levels in the cell body and ellipsoid. These results show photoreceptor Ca^{2+} homeostasis is controlled in a region-specific manner by direct Ca^{2+} entry and diffusion as well as Ca^{2+} extrusion. Moreover, quantitative measurement of $[Ca^{2+}]i$ levels in different photoreceptor compartments indicates that the dynamic range of Ca^{2+} signaling in photoreceptors is approximately 40-fold, from ~50 nM in the light to ~ 2 μM in darkness.

Key Words: retina, photoreceptor, Ca^{2+} channel, plasma membrane calcium ATPase, ellipsoid, TMRM

Introduction

The calcium ion is the most versatile known intracellular messenger, regulating almost all known cellular functions and processes (Berridge et al.,2003; Petersen et al., 2005). Changes in the intracellular calcium concentration, $[Ca^{2+}]i$, regulate cellular processes by activating diverse signaling pathways and organelles and by coordinating the amplitude and timing of Ca^{2+}-dependent processes across the cell. The distribution and abundance of Ca^{2+} channels, transporters and effector proteins creates local and/or global changes in $[Ca^{2+}]i$ (Berridge et al., 2003; Delmas et al., 2004). Such domain-specific action of Ca^{2+} is especially evident in primary sensory neurons, highly polarized cells formed by several anatomical domains with distinct functions (Zufall et al., 2000; Dumont et al., 2001; Krizaj and Copenhagen, 2002).

Rod and cone photoreceptors are highly compartmentalized neurons. For example, phototransduction is limited to the outer segment (OS), aerobic metabolism to the ellipsoid, gene expression and protein synthesis to the cell body, and exocytosis to the synaptic terminal. Apoptosis, a Ca^{2+}-dependent process that underlies most forms of photoreceptor degeneration, is initiated and develops in both the ellipsoid and the cell body (Doonan et al., 2003; Chiarini et al., 2003; Rohrer et al., 2004). All of these processes are regulated by light-evoked fluctuations in $[Ca^{2+}]i$ (Fain et al., 2001; Krizaj and Copenhagen, 2002). However, it is not understood how $[Ca^{2+}]i$ changes in different regions of the photoreceptor during stimulation, nor is it known whether and how different regions communicate via local Ca^{2+} fluxes. Moreover, there are significant inconsistencies in the literature regarding absolute $[Ca^{2+}]i$ levels, the dynamic range and the role for Ca^{2+} diffusion in rods and cones.

A key question in photoreceptor signaling is related to understanding the mechanisms that compress the 4-5 log unit dynamic range of phototransduction in the outer segment to the approximately 25-fold range for exocytosis in the photoreceptor terminal (Choi et al., 2005). Presynaptic $[Ca^{2+}]i$ represents the final common path for this signal compression. A recent study, focusing on Ca^{2+} regulation in synaptic terminals of salamander rods and cones, suggested that average $[Ca^{2+}]i$ in the terminal ranges from ~350 nM in hyperpolarized light-adapted cells to more than 39 μM in cells depolarized to

dark potentials (Steele et al., 2005). Other studies, however, proposed that this dynamic range of presynaptic average $[Ca^{2+}]i$ in photoreceptors extends from tens of nanomoles to submicromolar or low micromolar (Rieke and Schwartz, 1996; Thoreson et al., 2004). This discrepancy has significant implications for our understanding of regulation of exocytosis at ribbon synapses in darkness and light (e.g., Rieke and Schwartz, 1996; Thoreson et al., 2004 but see Kreft et al., 2003; Heidelberger et al., 1994).

Studies also diverge on the mechanisms of Ca^{2+} entry into photoreceptor cell body and ellipsoid regions. It has been suggested that at physiological 'dark' membrane potentials $[Ca^{2+}]i$ in cell bodies and ellipsoids of rods is close to baseline values characteristic of light-adapted cells (Steele et al., 2005). Consistent with this, immunolocalization studies report that Kv1.4 Ca^{2+} channels are expressed exclusively in presynaptic terminals (Morgans et al., 1998; Morgans 2001). On the other hand, other studies found that cell bodies of photoreceptors are also immunoreactive for subunits of voltage-activated Ca^{2+} channels (Nachman-Clewner et al., 1999; Morgans et al., 2001; Steele et al., 2005), suggestive of direct Ca^{2+} entry into these compartments.

To resolve these conflicting reports on Ca^{2+} dynamics in photoreceptor regions, we studied depolarization-evoked Ca^{2+} signals in post-OS domains of rods and cones. Our results show that voltage-gated Ca^{2+} influx at membrane potentials that mimic physiological depolarizations elevates $[Ca^{2+}]i$ from ~50 nM to ~2 μM in terminals. Our results also suggest that Ca^{2+} enters the ellipsoid and the cell body regions directly through local Ca^{2+} channels, with an additional potential component from diffusion. Finally, we find that the spatiotemporal $[Ca^{2+}]i$ gradient is correlated with the distribution of voltage-operated Ca^{2+} channels and PMCAs, which control the dynamic range of cytosolic $[Ca^{2+}]i$ in a region-specific manner. Our data suggests that interactions between plasma membrane Ca^{2+} entry and clearance mechanisms compress the 4-5 fold range of photon-evoked responses in the OS into a 20-fold dynamic range of presynaptic $[Ca^{2+}]i$.

Materials and Methods

Preparation of isolated cells: Larval stage tiger salamanders were decapitated and pithed using procedures approved by the UCSF Committee for Animal Care and in accordance with the National Institute of health Guide for the Care and Use of Laboratory Animals.

Dissociated photoreceptors were prepared following protocols described previously (Krizaj and Copenhagen, 1998). Briefly, retinas were dissected from enucleated eyes, and dissociated in 0 Ca^{2+} /papain (10 U/ml; Worthington, Freehold, NJ) saline for 20 min at room temperature (20-22^{o}C). The retina was cut into small pieces using a razorblade; each piece was dissociated separately immediately prior to the experiment. Cells were plated onto coverslips coated with 0.2 mg/ml concanavalin A (Sigma, St. Louis, MO). Although the salamander retina contains at least four classes of cones (Mariani, 1986), all cones studied here responded to pharmacological manipulations in an identical manner; the data obtained from different cone classes has therefore been tabulated together. The viability of isolated cone ellipsoids was tested by 30 sec incubation with 0.01% toluidine blue. The dye was excluded from isolated ellipsoids, suggesting that these subregions reseal and form viable compartments following dissociation. The recording chamber was superfused via two electronically controlled multi-inlet manifolds (MP-8, Warner Instruments). The control saline solution contained, in mM, 97 NaCl, 2 KCl, 2 $CaCl_2$, 2 $MgCl_2$, 10 HEPES, 2 lactic acid, 0.3 ascorbic acid and 1 taurine at 240 mOsm. pH was adjusted to 7.6 with NaOH. To stimulate glycolysis, the glucose concentration in all saline solutions was 20 mM (e.g., Winkler, 1981). All chemicals were obtained from Sigma.

$[Ca^{2+}]i$ measurements: These methods are fully described elsewhere (Krizaj and Copenhagen, 1998). Briefly, photoreceptors were loaded with 2-5 μM fura-2 AM (fura 2- acetoxymethylester; Molecular Probes, Eugene, OR) for 10 minutes and subsequently washed for 20 minutes. The fluorescence signals were acquired on an inverted microscope (Nikon Eclipse 200) using a dry 40x objective (N.A.= 0.8) or an oil 100x objective (N.A. = 1.2). Image acquisition was generally binned at 3x3 pixels (except for Fig. 2 where the binning was 2x2) and was run at 0.5-1 Hz by a cooled 12 bit digital CCD camera (Cascade, Photometrics, Tucson, AZ). The camera and the shutter (Lambda DG-4, Sutter Instruments, Novato, CA) were controlled by commercial software (Metafluor 6.1; Universal Imaging, West Chester, PA). Separate regions of interest (ROI) were defined that encompassed the synaptic terminal, cell body and ellipsoid regions. ROI size was ~4 μm^2 for the terminal, 20 μm^2 for the cell body, and 10 μm^2 for the ellipsoid. The proximity of the cell body and terminal in

cones generally precluded accurate estimation of cone terminal $[Ca^{2+}]i$, therefore the average $[Ca^{2+}]i$ elevations were measured in rod terminals with axons >5 μm in length. Emission ratios between the 340 nm and 380 nm excitation wavelengths were calculated after subtraction of the background fluorescence.

Free $[Ca^{2+}]$ levels were calibrated *in vivo* with 10 μM ionomycin in 0 and 10 mM $[Ca^{2+}]o$ saline using the standard relationship (Grzynkiewicz et al. 1985), and the K_d for Ca^{2+} binding to fura-2 was taken to be 224 nM (Almers and Neher, 1985; Neher, 1995). It is possible that the intracellular environment caused small changes in Ca^{2+} binding to fura-2, which would be expected to change errors in estimation of the Kd parameter (Grzynkiewicz et al. 1985). To test for potential compartmentalization of fura-2 dye within the mitochondria and other intracellular organelles, fura-2-loaded cells were depolarized with 20 mM KCl together with 2 mM Mn^{2+}. Greater than 95% of the ellipsoid fura-2 signal was quenched by exposure to Mn^{2+}, indicating that most of the dye was cytoplasmic (data not shown). The fura-2 dye, with a K_d of 224 nM, is ~90% saturated at ~ 2 μM $[Ca^{2+}]i$ (Augustine and Neher, 1992; Zhou and Neher, 1993), possibly resulting in an underestimation of $[Ca^{2+}]$ at > 2.5 μM. We were occasionally unable to calibrate $[Ca^{2+}]i$ levels; therefore, data for some cells is presented as 340/380 nm ratios. The decay time constants were calculated by fitting single exponentials to the decrease in $[Ca^{2+}]i$ following exposure to KCl (Krizaj and Copenhagen, 1998). $[Ca^{2+}]i$ rise times, which equal the rate of entry minus the rate of clearance, were estimated as the slope of the linear rising phase from the onset to peak of the $[Ca^{2+}]i$ elevation (Igor Pro, Wavemetrics, Lake Oswego, OR). All pooled data are presented as mean ± S.E.M. Significance was determined using the t-test.

For live staining, cells were labeled for 15 min in 0.5-1 μM solution of MitoTracker Red or 200 nM MitoTracker Green (Molecular Probes). MitoTracker Green contains a thiol-reactive chloromethyl moiety that results in stable peptide conjugates after accumulation in the mitochondria. The uptake of this probe is independent of the mitochondrial membrane potential. TMRM (tetramethylrhodamine), a cationic rhodamine-based dye that reversibly accumulates in the highly negatively charged mitochondrial matrix and fluoresces at negative membrane potentials, was used at 100 nM; dye loading was 30 min. Stock solutions of MitoTracker and TMRM dyes

were made in DMSO. TMRM fluorescence was analyzed using the linescan function of the confocal microscope at the 543 nm line (1%; LSM5 Pascal, Zeiss, Tarrytown NY).

Immunostaining: Immunostaining procedures were performed as described before (Krizaj et al., 2002). Retinal sections on slides were washed in PB for 15 min before permeabilization and blocking in 0.5% Triton X-100 and 10% goat serum. The antibodies used were raised against the α1 subunit of voltage-gated Ca^{2+} channels (Alomone ACC-004), Chemicon (MAB427); for PMCA labeling, Affinity BioReagents PMCA1 antibody (PA-914) was used at 1:100 dilution. Goat anti-mouse or goat anti-rabbit IgG (H+L) conjugated to fluorophores (Alexa 488 and Alexa 594 conjugates (Invitrogen), diluted 1:500 or 1:1000, were used as secondary antibodies. After incubation, sections on slides were washed in PB and mounted with Vectashield (Vector, Burlingame, CA). Negative controls for non-specific staining of secondary antibodies were performed for every set of experiments by omitting the primary antibodies. Immunofluorescent and differential interference contrast (DIC) images were acquired at depths of 12 bits on a confocal microscope using 488 nm Ar and 594 nm He/Ne lines for fluorophore excitation, suitable band-pass or long-pass filters for emission detection, and a 63x/0.9 NA water objective.

Results

Photoreceptor regions proximal to the OS – the ellipsoid, cell body and synaptic terminal – are uniquely defined by their morphology (Fig. 1; Mercurio and Holtzman, 1982; Nilsson, 1985; Townes-Anderson et al., 1985). The aim of this report is to determine the dynamic range of $[Ca^{2+}]i$ in the different regions of hyperpolarized and depolarized photoreceptors to obtain a basis for understanding how Ca^{2+} regulates diverse signaling pathways in light and darkness, respectively. Moreover, we find that Ca^{2+} influx into cell bodies and ellipsoids occurs via indigenous local voltage-operated Ca^{2+} channels.

---Figure 1 near here---

Depolarization-evoked Ca^{2+} signals have a distinct spatiotemporal pattern

The spatial and temporal dynamics of depolarization-evoked $[Ca^{2+}]i$ responses in salamander photoreceptor non-OS regions were studied with functional Ca^{2+} imaging. Rods and cones were freshly isolated and loaded with the Ca^{2+} indicator dye fura-2 AM. The baseline $[Ca^{2+}]i$ in all non-OS regions of rod photoreceptors was under 100 nM (synaptic terminal, 98 ± 24 nM; cell body, 57 ± 7 nM; ellipsoid, 56 ± 5 nM). Cells were depolarized by superfusion with elevated concentrations of KCl (high K^+). Depolarization-evoked $[Ca^{2+}]i$ exhibited a highly reproducible standing $[Ca^{2+}]i$ gradient across the terminal, cell body, and ellipsoid (Fig. 2). A representative experiment showing the effects of depolarization on photoreceptor $[Ca^{2+}]i$ domains is illustrated in Fig. 2.

---Figure 2 near here---

A statistical analysis summarizing the amplitudes of $[Ca^{2+}]_i$ elevations evoked by 30 mM KCl in the terminal, cell body and ellipsoid is shown in Fig. 3. The amplitude of depolarization-evoked $[Ca^{2+}]_i$ increases in rod terminals was 2160 ± 196 nM (n=5). $[Ca^{2+}]i$ elevations occurred at discrete puncta within the terminal, raising average $[Ca^{2+}]i$ within the terminal above 2 μM (Fig. 2B & C). The increases were significantly lower in the cell body (1168 ± 87 nM; $P<0.005$; n=19) and were sharply delimited from the subellipsoid, an endoplasmic reticulum-rich space that separates the cell body from the ellipsoid (Fig. 2B). By far the lowest concentration and the slowest kinetics of evoked responses were observed in the ellipsoid (754 ± 55 nM, n=19) (Figs. 2A & 3).

The gradient of depolarization-evoked $[Ca^{2+}]i$ across the cell was stable for the duration of the experiment. The region-specific amplitude and kinetics of depolarization-evoked $[Ca^{2+}]i$ pattern illustrated in Figures 2 & 3 were observed in all intact cells and were highly conserved across rods and all subtypes of cones. The differences between cell regions were statistically significant ($P<0.001$ to $P<0.005$). In cells lacking synaptic terminals, Ca^{2+} signals were first observed in the cell body domain closest to the axon, possibly as a result of higher density of Ca^{2+} channel expression in this region or due to retraction of the Ca^{2+} channel-rich terminal into the soma (data not shown; Townes-Anderson et al. 1985, but see Nachman-Clewner et al., 1999; Steele et al., 2005).

These results show that depolarization evokes micromolar increases in global $[Ca^{2+}]i$ in rod terminals and submicromolar changes in perikaryal and ellipsoid $[Ca^{2+}]i$. Below we analyze the mechanisms responsible for controlling the amplitude and kinetics of depolarization-evoked responses.

--- Figure 3 near here---

Depolarization triggers direct Ca^{2+} influx into the photoreceptor cell body

A recent report using optical imaging suggested that, following stimulation with 30 mM KCl, there is at least a 250-fold difference between the amplitude of depolarization-evoked $[Ca^{2+}]i$ responses in the soma and the terminal of rods (Steele et al., 2005). This study suggested that under physiological conditions $[Ca^{2+}]$ elevations in the cell body would occur via diffusion from the synaptic terminal. The same study, however, found the apparent intensity of immunostaining for α_{1D} subunit-containing L-type Ca^{2+} channels to be only ~three-fold higher within the terminal compared to the soma (Steele et al., 2005). To address this discrepancy, and to determine the fraction of Ca^{2+} entering the cell body by diffusion, we recorded Ca^{2+} responses from rods with and without terminals. If most perikaryal $[Ca^{2+}]i$ is due to Ca^{2+} diffusion from the terminal, then depolarization should evoke little response in rods in which synaptic terminals had been cut off experimentally. In contrast, if cell bodies express functional voltage-operated Ca^{2+} channels, depolarization-evoked responses should be detected in axotomized cells. The terminals were cut in 0 Ca^{2+} saline with a sharp microelectrode (Fig. 4A, B). Following a resealing period of 15-30 minutes, cells were returned to control saline and $[Ca^{2+}]i$ responses measured in 30 mM KCl. As illustrated in Figure 4D, cell bodies in control and axotomized cells had comparable $[Ca^{2+}]i$ baselines of 71 ± 20 nM for controls and 79 ± 29 for axotomized cells. High K^+ raised $[Ca^{2+}]i$ by 988 ± 83 nM in 4 out of 5 axotomized rods, not significantly different from 1168 ± 255 nM measured in intact cells (n=19; P=0.0656; Figures 3 and 4C, D). In cells possessing intact synaptic terminals, perikaryal $[Ca^{2+}]i$ responses were 1250 ± 253 (n=5), not significantly different from axotomized rods (P=0.1086). A small (45 nM) $[Ca^{2+}]i$ elevation was detected in the cell body of 1/5 axotomized cells; this cell body had a relatively high basal $[Ca^{2+}]i$ of 100

nM. This data is strongly suggestive of endogenous voltage-operated Ca^{2+} channels in cell bodies of photoreceptors.

--- Figure 4 near here---

$[Ca^{2+}]$i regulation in the photoreceptor ellipsoid

To determine whether the ellipsoid $[Ca^{2+}]$i elevation exemplified in Fig 2 could result from Ca^{2+} influx through local plasma membrane channels, depolarization-evoked $[Ca^{2+}]$i responses were analyzed in isolated ellipsoids. These experiments were performed in cones, because it was possible to separate cone, but not rod, ellipsoids mechanically from perikarya. Three types of control experiment were performed to determine the viability and integrity of isolated cone ellipsoids. First, exposure to the vital dye toluidine blue showed that isolated ellipsoids exclude the dye, suggesting that ellipsoid membrane maintains its integrity following dissociation (Fig. 5A). Second, cells were labeled simultaneously with TMRM (100 nM), a cationic rhodamine-based dye that reversibly accumulates in the highly negatively charged mitochondrial matrix (Scaduto and Grotyohann, 1999), and MitoTracker Green (200 nM), a mitochondria-specific indicator that is independent of the membrane potential (Pendergrass et al., 2004). We reasoned that if mitochondrial function in the isolated ellipsoid is normal, the MitoTracker Green signal should occupy the same area as TMRM. Indeed, complete superposition between TMRM and Mitotracker Green signals was observed in intact ellipsoids (Fig. 5Bi,Bii). The intensity of the TMRM signal was identical in isolated and intact ellipsoids (Fig. Bi; n=9 pairs). We additionally tested the mitochondrial membrane potential by exposing cells to the mitochondrial uncoupler antimycin. Following application of 8 μM antimycin, the intensity of the TMRM signal in isolated and intact ellipsoids decreased with a time constant of ~6.6 min (Fig. 5C, D). These results suggest that the mitochondrial membrane potential in isolated ellipsoids is normal. The baseline $[Ca^{2+}]$i in isolated ellipsoids was slightly elevated (58.18 ± 8.92 nM) with respect to controls (45 ± 4.83 nM); however, this difference was not significant (P=0.2775). Taken together, these four control experiments indicate that following dissociation the isolated ellipsoid remains a structurally and functionally intact compartment.

--- Figure 5 near here---

L-type channel blockers suppress depolarization-evoked $[Ca^{2+}]i$ responses in both cell body and ellipsoid of the intact cell (Fig. 6A). To test whether Ca^{2+} entry occurs directly into the ellipsoid itself, evoked responses were analyzed in isolated ellipsoids. Stimulation with high K^+ induced significant $[Ca^{2+}]i$ elevations in isolated ellipsoids (Fig. 3). To amplify depolarization-evoked responses from isolated ellipsoids, KCl concentration in a subset of experiments was raised to 60 mM. Superfusion with 60 mM KCl increased isolated ellipsoid $[Ca^{2+}]_i$ from 33 ± 7 nM to 586 ± 131 nM (n=4; Fig. 6B). In the presence of nifedipine, depolarization elevated $[Ca^{2+}]_{ellipsoid}$ by only ~33 nM (from 48 ± 9 to 81 ±13 nM; Fig. 6B), suggesting ellipsoids express functional L-type Ca^{2+} channels. In control experiments, 60 mM KCl elevated $[Ca^{2+}]i$ in ellipsoids and cell bodies of intact cones to 1407 ± 320 nM and 3117 ± 349 nM, respectively (Fig. 3). This data shows that responses from isolated ellipsoids are roughly about half the elevations observed in intact ellipsoids and five-fold lower than increases in the cell body.

--- Figure 6 near here---

If diffusion provides a component of the depolarization-evoked $[Ca^{2+}]i$ signal within the ellipsoid, the rate of Ca^{2+} increase ($d[Ca^{2+}]i/dt$) within isolated ellipsoids should be slower compared to ellipsoids in intact cells. Figure 7A shows the time course of depolarization-evoked $[Ca^{2+}]i$ elevations recorded from the an intact cell body and its attached ellipsoid, and an isolated cone ellipsoid. The rise-time and decay constant of depolarization-evoked Ca^{2+} transients in isolated ellipsoids was almost three-fold slower than in ellipsoids from intact cones (Fig. 7).

Assuming intracellular [K+] in amphibian excitable cells to be ~124 mM (Aidley, 1989), 30 mM and 60 mM KCl depolarized ellipsoids to –36 mV and –18 mV, respectively. Doubling $[K^+]o$ increased $[Ca^{2+}]i$ in intact ellipsoids by 211 ± 23%, compared to 164 ± 22% in isolated ellipsoids. Interestingly, while doubling the concentration of extracellular K^+

caused an approximately six-fold increase in the rate of $[Ca^{2+}]_i$ rise in the cell body, only a two-fold increase was observed in the intact ellipsoid (Fig. 7C, E).

Unlike the cell body, which responded to the increase in extracellular K^+ with an increase in the rate of Ca^{2+} clearance (the time constant decreased from 20 ± 4 to 10 ± 5 sec), an equivalent increase in $[Ca^{2+}]_i$ clearance was not observed in the ellipsoid of intact cone photoreceptors (24 ± 4 to 19 ± 3sec) nor in the isolated ellipsoid (32 ± 4 to 35 ± 11 sec) (Fig. 5C). This data suggests that Ca^{2+} enters the ellipsoid via local Ca^{2+} channels, with a possible additional diffusion component from the cell body. The kinetics of onset and offset of depolarization-evoked $[Ca^{2+}]$i signals in the ellipsoid were greatly reduced vis a vis the cell body, consistent with low expression levels of plasma membrane Ca^{2+} channels and pumps (see below) and Ca^{2+} sequestration into intracellular compartments such as the mitochondria (Krizaj et al., 2003).

--- Figure 7 near here ---

Expression of Ca^{2+} influx and extrusion mechanisms in the IS is consistent with spatiotemporal dynamics of depolarization-evoked Ca^{2+} signals

We next tested whether spatiotemporal variation in depolarization-evoked signals in photoreceptors could be attributed to differential distribution of Ca^{2+} channels and PMCA pumps within the non-OS region. Since the identity of Ca^{2+} channels in salamander photoreceptors has not yet been unequivocally established, we immunostained salamander retinal sections with antibodies raised against the consensus sequence common to all L type α_1 Ca^{2+} channel subunits. Prominent α_1 subunit immunofluorescence was observed in synaptic terminals in the outer plexiform layer (OPL) (Fig. 8B, arrows) and the inner plexiform layer (not shown). Müller cell processes enveloping photoreceptors and throughout the retina were α_1-immunoreactive. At higher confocal gains, the pan-α_1 signal was observed in the cell body of rods and cones, consistent with sparser Ca^{2+} channel expression. In contrast, little Ca^{2+} channel expression in the ellipsoid area was seen using this antibody.

We also attempted to correlate the kinetics of Ca^{2+} decay following depolarization with expression of the dominant plasma membrane Ca^{2+} clearance mechanism in

photoreceptors. Ca^{2+} extrusion in salamander photoreceptors is supported exclusively by plasma membrane Ca^{2+} ATPases (PMCAs; Krizaj and Copenhagen, 1998). A recent analysis of PMCA expression in the salamander retina showed that salamander rods and cones express PMCA isoforms 1, 2 and 4 (Krizaj et al., 2004); however, a region-specific analysis was not performed in that study. The salamander retina was immunostained with the antibody PMCA1, the dominant PMCA isoform in vertebrate photoreceptors (Krizaj et al., 2002). As illustrated in Figure 8D, the antibody strongly labeled photoreceptor terminals, with a moderate expression in the cell body. These results suggest that high rate of Ca^{2+} clearance from the synaptic terminal observed physiologically (Krizaj and Copenhagen, 1998) reflects the high PMCA density in synaptic terminals of rods and cones.

--- Figure 8 near here---

Discussion

In darkness, photoreceptors are tonically depolarized, resulting in sustained entry of Ca^{2+} and elevation of $[Ca^{2+}]i$. The aim of this study was to characterize the spatiotemporal pattern of elevated free $[Ca^{2+}]i$ in the three non-phototransducing regions of depolarized rods and cones and to determine the dynamic range of physiological Ca^{2+} concentrations across photoreceptor regions. Using optical imaging we show that (1) Depolarization is associated with a standing $[Ca^{2+}]i$ gradient across non-OS regions of rod and cone photoreceptors. This gradient is produced in part by polarized expression of Ca^{2+} channels and pumps (2) Ca^{2+} entry into the cell body and ellipsoid occurs via indigenous Ca^{2+} channels with a minor contribution from Ca^{2+} diffusion. (3) Physiological depolarization evokes micromolar increases in terminal $[Ca^{2+}]i$ with ~40-fold dynamic range.

Spatiotemporal Ca^{2+} gradient within the photoreceptor inner segment

The amplitude of depolarization-evoked $[Ca^{2+}]_i$ signals in rod photoreceptor synaptic terminal is ~double those in the cell body and ~2.5-fold higher than in the ellipsoid (Figs. 2 and 3) whereas the rates of Ca^{2+} entry and extrusion were 1.5-3-fold

higher for the cell body compared to the ellipsoid. The gradient of depolarization-evoked $[Ca^{2+}]i$ across the cell was remarkably stable for the duration of the experiments (>1hr) and could have originated either from Ca^{2+} influx from the extracellular space or Ca^{2+} release from intracellular Ca^{2+} stores. The dihydropyridine blocker nifedipine suppressed depolarization-evoked Ca^{2+} signals in all non-OS regions, suggesting most voltage-activated Ca^{2+} influx occurs via the L-type class of Ca^{2+} channel. Consistent with this, the $[Ca^{2+}]i$ gradient correlated with the expression levels of L-type Ca^{2+} channels and PMCA pumps (Fig. 8; Krizaj et al., 2004; see also Nachman-Clewner et al., 1999, Morgans 2001). The pattern of depolarization-evoked $[Ca^{2+}]i$ signals in cones was similar to the responses observed in rods. The additional advantage of the cone preparation was that it allowed us to directly study Ca^{2+} entry pathways in the ellipsoid region (see below).

The data presented suggests that at physiological depolarizations the average $[Ca^{2+}]i$ within photoreceptor terminals of rods spans the operating range from 50-100 nM in the light to ~ 2 μM in darkness. Assuming ~60 channels are open in a salamander rod terminal at the dark resting potential (Heidelberger et al., 2005) and an average number of 7.3 Ca^{2+} channel clusters that produce $[Ca^{2+}]i$ hotspots per terminal (Nachmann-Clewner et al., 1999), each hotspot at dark membrane potentials would have ~ 8 open channels and contribute ~287 nM free Ca^{2+} within an area of ~0.76 um^2. While we did detect local elevations in terminal $[Ca^{2+}]i$ (Figure 2B), the relationship between exocytosis and localized increases in terminal $[Ca^{2+}]i$ remains to be studied. However, our data shows that photoreceptors compress the 4-5 log unit dynamic range obtained by the phototransduction cascade in the OS (Schnapf et al., 1990; Fain et. al. 2001) into a 20-fold operating range of $[Ca^{2+}]i$ within the presynaptic terminal. This resembles the 28-fold range for exocytosis in synaptic terminals of cones (Choi et al., 2005) and suggests that photoreceptor output is controlled by Ca^{2+} homeostatic mechanisms within the terminal. Thus presynaptic gain control by Ca^{2+} extrusion, release from stores (Krizaj et al., 1999; 2003), neuromodulation (Stella et al. 2002) and feedback from horizontal cells (Verweij et al., 1996; Vessey et al., 2005) may mediate presynaptic adaptation via regulation of terminal $[Ca^{2+}]$.

Our results differ from the recently reported data that suggested $[Ca^{2+}]i$ baseline in synaptic terminals of light adapted rods is ~350 nM, exceeding 39 μM during

depolarization with 30 mM KCl (Steele et al. (2005). The conclusions reached by Steele et al. are difficult to interpret given that the fura-2 dye used in that study saturates at 2-3 μM $[Ca^{2+}]i$ (Neher 1995). Furthermore, the relative Ca^{2+} concentrations in different cell regions in Steele et al. (2005) are difficult to extrapolate because cell regions were not calibrated in situ.

Immunocytochemical studies of Ca^{2+} channel expression in photoreceptors have been equivocal. In rat photoreceptors, L-type Ca^{2+} immunoreactivity with antibodies against the retina-specific α_{1F} subunit showed strong signal within the synaptic terminal whereas the signal in the cell body and the ellipsoid was undetectable (Morgans et al., 1998; Morgans 2001). However, other antibodies raised against the α_{1F} subunit showed more prominent immunostaining of the ONL (Morgans et al., 2001 suggesting the possibility that different Ca^{2+} channel isoforms are expressed within different non-OS compartments. Immunostaining of dissociated salamander photoreceptors with α_{1C} subunit antibodies showed equally prominent immunostaining in the cell body and the synaptic terminal of rods and cones whereas little α_{1C}, signal was detected in the ellipsoid (Nachman-Clewner et al., 1999). However, an α_{1D} antibody appeared to stain terminals of dissociated salamander rods about 3-fold more strongly than cell bodies, in contrast to the difference observed with Ca^{2+} imaging (Steele et al., 2005). Given the difficulty of quantifying the absolute densities of antigens in immunostained sections and the questions about the α_1 subunits expressed in salamander photoreceptors (Nachman-Clewner et al., 1999; Steele et al., 2005) we performed qualitative immunostaining of retinal sections with pan Ca^{2+} channel antibodies recognizing all α_1 isoforms. Our results suggest that (i) Voltage-operated Ca^{2+} channels are expressed at low densities in somas of rods and cones, consistent with direct Ca^{2+} entry into the soma, and (ii) The ellipsoid membrane contains Ca^{2+} channels at a density that is below the resolution of our antibody staining.

Consistent with low L type Ca^{2+} channel immunoreactivity in the ellipsoid (Fig. 8; see also Morgans et al., 1998; Nachman-Clewner et al., 1999), a recent report suggested that depolarization with 30 mM KCl evokes little or no response from cell bodies and ellipsoids of rods (Steele et al., 2005). We took the advantage of the high sensitivity of functional Ca^{2+} imaging to show directly that depolarization increases

$[Ca^{2+}]i$ in both isolated cell bodies and ellipsoids. In our experiments, depolarization-evoked $[Ca^{2+}]i$ increases were observed in axotomized cell bodies and in dissociated ellipsoids, suggesting that both regions express indigenous voltage-operated Ca^{2+} channels activated at dark potentials (~-35 mV in 30 mM KCl). Taken together, more than 95% of rod cell bodies, with and without visible axons, and including axotomized cells, were responsive to 20 mM and 30 mM KCl ($n >> 150$, including data from Krizaj and Copenhagen 1998; 1999; Krizaj et al., 2003).

There is increasing evidence that somatic $[Ca^{2+}]$ is not only controlled by plasma membrane Ca^{2+}-permeable channels but also by intracellular stores (Gerasimenko and Gerasimenko, 2004; Krizaj and Szikra unpublished observations). Calcium-induced Ca^{2+} release, which may contribute up to 40% to the depolarization-evoked Ca^{2+} signal within the cell body (Krizaj et al., 2003), could also contribute to the discrepancy between the relatively weak expression of L-type Ca^{2+} channels observed with immunostaining and prominent $[Ca^{2+}]i$ elevations observed in physiological experiments. The mean amplitude of depolarization-evoked $[Ca^{2+}]i$ increases in the cell body of axotomized cells was ~80% of those observed in intact cells (Figures 2 - 4). It is possible that Ca^{2+} diffusion from the terminal into the cell body plays a larger role at higher depolarization levels (Steele et al., 2005).

A potential explanation for the low amplitude and slow time course of Ca^{2+} signals within the ellipsoid might lie in compartmentalization of fura-2 dye within the mitochondria. However, >95% of the ellipsoid fura-2 signal was quenched by exposure to Mn^{2+}, indicating that most of the dye was cytoplasmic (data not shown). We propose that the ellipsoid plasma membrane contains a low density of Ca^{2+} channels at a density that is below the resolution of our antibody staining. Interestingly, the mean amplitudes and kinetics of depolarization-evoked Ca^{2+} elevation and decay in isolated ellipsoids were consistently ~50% of those in intact ellipsoids. Although this could be attributed to damage during the isolation procedure, we found that isolated ellipsoids excluded vital dyes such as toluidine blue and appeared to have inner mitochondrial membrane potentials indistinguishable from those in intact cells. Moreover, baseline $[Ca^{2+}]i$ levels in isolated ellipsoids were not statistically different from $[Ca^{2+}]i$ levels in intact ellipsoids, arguing against increased Ca^{2+}-mediated inactivation of Ca^{2+} entry in the former. Finally,

the doubling of extracellular KCl resulted in supralinear increase in ellipsoid $[Ca^{2+}]i$. Although at the moment there is no direct evidence for intra-compartmental Ca^{2+} diffusion or its potential modulation by intracellular stores and PMCAs in rods and cones, the (a) $[Ca^{2+}]$-dependence of the Ca^{2+} diffusion coefficient (Allbritton et al., 1992), (b) gradient of expression of voltage-operated Ca^{2+} channels and PMCAs in the inner segment and (c) a large potential Ca^{2+} sink represented by the ellipsoid mitochondria (Fig. 5), lead us to hypothesize that Ca^{2+} diffusion from the cell body towards an ellipsoid sink might additionally contribute to the inter-regional $[Ca^{2+}]i$ gradient in depolarized cells.

Functional implications of the spatiotemporal $[Ca^{2+}]i$ gradient

The separation of distinct Ca^{2+} signaling mechanisms in spatial domains of a photoreceptor is well suited for photoreceptor signaling. $[Ca^{2+}]i$ levels in the OS determine the rate and extent of adaptation to light (Fain et al., 2001). To preserve the fidelity of the light response, it is imperative to protect the gain control mechanisms in the OS from interference by Ca^{2+} fluxes in the inner segment. This may be especially important for cones, as baseline $[Ca^{2+}]i$ in saturated light-adapted cone OSs is several-fold lower (~ 5 nM; Sampath et al., 1999) compared to inner segment $[Ca^{2+}]i$ (~20-40 nM). The low density of voltage-operated Ca^{2+} channels and Ca^{2+} sequestration by its resident mitochondria (Nilsson 1985; Townes-Anderson et al., 1985; Hoang et al., 2002; Krizaj et al., 2003) ensure that the ellipsoid serves as a buffer for Ca^{2+} fluxes between the OS and the rest of the cell. Consistent with a mitochondrial Ca^{2+} sink within the ellipsoid (Szikra and Krizaj, 2005), the kinetics of Ca^{2+} signals in the ellipsoid was slow and independent of doubling of [KCl]o (Fig. 5). Why are voltage-operated Ca^{2+} channels expressed in the ellipsoid at all? Photoreceptors are among the biggest energy consumers in the brain (Stone et al., 1999). Mitochondria undergo large changes in matrix $[Ca^{2+}]i$ following Ca^{2+} influx via plasma membrane Ca^{2+} channels (Rutter et al., 1993; Babcock et al., 1997). In turn, the amplitude of the Ca^{2+} rise inside the mitochondria determines the increases in cytosolic and mitochondrial ATP concentrations (Fein and Tsacopoulos, 1988; McCormack et al., 1990; Jouaville et al., 1999). We propose that Ca^{2+} diffusion

from the cell body does not provide adequate stimulation of mitochondrial dehydrogenases needed to sustain the metabolic needs of photoreceptors.

The large depolarization-evoked Ca^{2+} signals in the cell body may play a role in nuclear gene activation (Dolmetsch et al., 2001). The c-fos promoter, which appears to be able to selectively respond to changes in cytoplasmic and nuclear $[Ca^{2+}]i$ would be a prime candidate here (Hardingham et a., 1997; Grimm et al., 2000). There is increasing evidence that somatic $[Ca^{2+}]$ is controlled by both plasma membrane Ca^{2+}-permeable channels and intracellular stores (Hardingham et a., 1997; Gerasimenko and Gerasimenko, 2004). Ca^{2+} release from perikaryal stores is likely to additionally amplify the depolarization-evoked signal amplitude and thus influence gene expression (Mao and Wang, 2003; Carrasco et al., 2004; see also Marius et al., 2006). Ryanodine, $InsP_3$ receptors and SERCA transporters are expressed in the cell body and terminal but not the ellipsoid regions (Krizaj et al., 2004), consistent with the observations of caffeine-evoked $[Ca^{2+}]i$ signals in the cell body and the terminal (Krizaj et al., 1999). Finally, high density of L-type channels in the terminal is well suited for controlling rapid and reliable exocytosis. The high surface-to-volume ratio of the synaptic terminal and high density of PMCAs are likely to limit fast high amplitude $[Ca^{2+}]i$ signals to the terminal, ensuring that $[Ca^{2+}]i$ levels and the exocytotic rate drop rapidly during the light onset. Parenthetically, a compartmentalized pattern of Ca^{2+} channels, Ca^{2+} store transporters and PMCA expression was also reported for retinal bipolar cells and cochlear/vestibular hair cells (Dumont et al., 2001; Krizaj et al., 2002). In bipolar cells, depolarization triggers compartmentalized $[Ca^{2+}]i$ elevations (Heidelberger and Matthews, 1992) that mirror those observed in photoreceptors. For example, slow low-amplitude depolarization-evoked signals in bipolar cell bodies were observed seen following severance of the synaptic terminal, indicating expression of indigenous voltage-operated Ca^{2+} channels (Heidelberger and Matthews, 1992).

In conclusion, we determined the amplitude and kinetics of $[Ca^{2+}]i$ signals in different regions of the photoreceptor cell and ascertained the contribution of endogenous voltage-operated Ca^{2+} channels in the cell body and ellipsoid regions. Our results underscore the importance of careful analysis of Ca^{2+} dynamics in photoreceptor compartments when using ratiometric Ca^{2+} indicators. We hypothesize that $[Ca^{2+}]i$ can be

independently controlled between the outer and inner segment, and between different non-OS domains of rods and cones, allowing for intricate local modulation by separate and distinct Ca^{2+}-dependent signaling pathways.

Grants: This work was supported by a grant from the Hungarian Eötvös Fellowship and The Knights Templar Foundation to T.Sz., by the National Institutes of Health (EY13870), That Man May See Foundation to D.K. and an unrestricted grant from Research to Prevent Blindness to the UCSF Dept. of Ophthalmology. D.K. is a Research to Prevent Blindness James S. Adams Scholar. We thank Dr. Rene Rentería for helpful comments.

References:

Akopian A and Witkovsky P (2002) Calcium and retinal function. Molecular Neurobiology. 25:113-132.

Allbritton NL, Meyer T, Stryer L (1992) Range of messenger action of calcium ion and inositol 1,4,5-trisphosphate. Science. 258:1812-1815.

Augustine GJ, Neher E (1992) Neuronal Ca^{2+} signalling takes the local route. Curr Opin Neurobiol. 2:302-307.

Almers W, Neher E (1985) The Ca signal from fura-2 loaded mast cells depends strongly on the method of dye-loading. FEBS Lett. 192:13-18.

Berridge MJ, Bootman MD, Roderick HL (2003) Calcium signalling: dynamics, homeostasis and remodelling. Nat Rev Mol Cell Biol 4:517-529.

Carrasco MA, Jaimovich E, Kemmerling U, Hidalgo C (2004) Signal transduction and gene expression regulated by calcium release from internal stores in excitable cells. Biol Res. 37:701-712.

Chiarini LB, Leal-Ferreira ML, de Freitas FG, Linden R (2003) Changing sensitivity to cell death during development of retinal photoreceptors. J Neurosci Res. 74:875-883.

Choi SY, Borghuis B, Rea R, Levitan ES, Sterling P, Kramer RH (2005) Encoding light intensity by the cone photoreceptor synapse. Neuron 48:555-562.

Delmas P, Crest M, Brown DA (2004) Functional organization of PLC signaling microdomains in neurons. Trends Neurosci 27:41-47

Dolmetsch RE, Pajvani U, Fife K, Spotts JM, Greenberg ME (2001) Signaling to the nucleus by an L-type calcium channel-calmodulin complex through the MAP kinase pathway. Science 294:333-39.

Doonan F, Donovan M, Cotter TG (2003) Caspase-independent photoreceptor apoptosis in mouse models of retinal degeneration. J Neurosci. 23:5723-5731.

Dumont RA, Lins U, Filoteo AG, Penniston JT, Kachar B, Gillespie PG (2001) Plasma membrane Ca^{2+}-ATPase isoform 2a is the PMCA of hair bundles. J Neurosci 21:5066-5078.

Fein A, Tsacopoulos M (1988) Activation of mitochondrial oxidative metabolism by calcium ions in Limulus ventral photoreceptor. Nature. 331:437-440.

Fain GL, Matthews HR, Cornwall MC, Koutalos Y (2001) Adaptation in vertebrate photoreceptors. Physiol Rev. 81:117-151.

Gerasimenko O, Gerasimenko J (2004) New aspects of nuclear calcium signalling. J Cell Sci. 117:3087-3094.

Grimm C, Wenzel A, Hafezi F, Reme CE (2000) Gene expression in the mouse retina: the effect of damaging light. Mol Vis. 6:252-260.

Grynkiewicz G, Poenie M, Tsien RY (1985) A new generation of Ca^{2+} indicators with greatly improved fluorescence properties. J Biol Chem. 260:3440-3450

Holtzman E, Mercurio AM. 1980. Membrane circulation in neurons and photoreceptors: some unresolved issues. Int Rev Cytol 67:1-67.

Hardingham GE, Chawla S, Johnson CM, Bading H (1997) Distinct functions of nuclear and cytoplasmic calcium in the control of gene expression. Nature 385:260-265.

Heidelberger R, Matthews G (1992) Calcium influx and calcium current in single synaptic terminals of goldfish retinal bipolar neurons. J Physiol. 447:235-235

Heidelberger R, Heinemann C, Neher E, Matthews G (1994) Calcium dependence of the rate of exocytosis in a synaptic terminal. Nature. 371:513-515.

Heidelberger R, Thoreson WB, Witkovsky P (2005) Synaptic transmission at retinal ribbon synapses. Prog Retin Eye Res. 24:682-720.

Hoang QV, Linsenmeier RA, Chung CK, Curcio CA (2002) Photoreceptor inner segments in monkey and human retina: mitochondrial density, optics, and regional variation. Vis Neurosci 19:395-407.

Jouaville LS, Pinton P, Bastianutto C, Rutter GA, Rizzuto R (1999) Regulation of mitochondrial ATP synthesis by calcium: evidence for a long-term metabolic priming. Proc Natl Acad Sci U S A. 96:13807-13812.
Kreft M, Krizaj D, Grilc S, Zorec R (2003) Properties of exocytotic response in vertebrate photoreceptors. J Neurophysiol. 90:218-225.
Krizaj D, Copenhagen DR (1998) Compartmentalization of calcium extrusion mechanisms in the outer and inner segments of photoreceptors. Neuron 21:249-256.
Krizaj D, Bao JX, Schmitz Y, Witkovsky P, Copenhagen DR (1999) Caffeine-sensitive calcium stores regulate synaptic transmission from retinal rod photoreceptors. J Neurosci. 19:7249-7261.
Krizaj D, Copenhagen DR (2002) Calcium regulation in photoreceptors. Front Biosci 7:d2023-d2044.
Krizaj D, Lai FA, Copenhagen DR (2003) Ryanodine stores and calcium regulation in the inner segments of salamander rods and cones. J Physiol 547:761-774.
Krizaj D, Liu X, Copenhagen DR (2004) Expression of calcium transporters in the retina of the tiger salamander (Ambystoma tigrinum). J Comp Neurol 475:463-480.
Mao L, Wang JQ. (2003) Group I metabotropic glutamate receptor-mediated calcium signalling and immediate early gene expression in cultured rat striatal neurons. Eur J Neurosci. 17:741-750.
Mariani AP (1986) Photoreceptors of the larval tiger salamander retina. Proc R Soc Lond B Biol Sci 227: 483-492.
Marius P, Guerra MT, Nathanson MH, Ehrlich BE, Leite MF (2006) Calcium release from ryanodine receptors in the nucleoplasmic reticulum. Cell Calcium. 39:65-73..
Mercurio AM, Holtzman E (1982) Smooth endoplasmic reticulum and other agranular reticulum in frog retinal photoreceptors. J Neurocytol 11:263-293.
Morgans CW, El Far O, Berntson A, Wässle H, Taylor WR (1998) Calcium extrusion from mammalian photoreceptor terminals. J Neurosci 18:2467-2474.
Morgans CW (2001) Localization of the alpha(1F) calcium channel subunit in the rat retina. Invest Ophthalmol Vis Sci 42:2414-2418.
Nachman-Clewner M, St Jules R, Townes-Anderson E (1999) L-type calcium channels in the photoreceptor ribbon synapse: localization and role in plasticity. J Comp Neurol.

415:1-16.
Nakatani K, Chen C, Koutalos Y (2002) Calcium diffusion coefficient in rod photoreceptor outer segments. Biophys J 82:728-39.
Neher E (1995) The use of fura-2 for estimating Ca buffers and Ca fluxes. Neuropharmacology 34:1423-1442.
Neher E, Augustine GJ. (1992) Calcium gradients and buffers in bovine chromaffin cells. J Physiol. 450:273-301.
Nilsson SE (1985) The retinal photoreceptors and the pigment epithelium. Structure and function. Transduction. Acta Ophthalmol Suppl 173:4-8.
Pendergrass W, Wolf N, Poot M (2004) Efficacy of MitoTracker Green and CMX rosamine to measure changes in mitochondrial membrane potentials in living cells and tissues. Cytometry 61:162-169.
Petersen OH, Michalak M, Verkhratsky A (2005) Calcium signaling: Past, present and future. Cell Calcium 38: 161-169.
Rieke F, Schwartz EA (1996) Asynchronous transmitter release: control of exocytosis and endocytosis at the salamander rod synapse. J Physiol. 493:1-8.
Rohrer B, Pinto FR, Hulse KE, Lohr HR, Zhang L, AlmeidaJS (2004) Multidestructive pathways triggered in photoreceptor cell death of the rd mouse as determined through gene expression profiling. J Biol Chem. 279:41903-41910.
Rutter GA, Theler JM, Murgia M, Wollheim CB, Pozzan T, Rizzuto R (1993) Stimulated Ca^{2+} influx raises mitochondrial free Ca^{2+} to supramicromolar levels in a pancreatic beta-cell line. J Biol Chem. 268:22385-22390
Satoh H, Aoki K, Watanabe SI, Kaneko A (1998) L-type calcium channels in the axon terminal of mouse bipolar cells. Neuroreport 9:2161-2165.
Stella SL Jr, Bryson EJ, Thoreson WB (2002) A2 adenosine receptors inhibit calcium influx through L-type calcium channels in rod photoreceptors of the salamander retina. J Neurophysiol. 87:351-360.
Scaduto RC Jr, Grotyohann LW (1999) Measurement of mitochondrial membrane potential using fluorescent rhodamine derivatives. Biophys J. 76:469-477.
Steele EC Jr, Chen X, Iuvone PM, MacLeish PR (2005) Imaging of Ca^{2+} dynamics within the presynaptic terminals of salamander rod photoreceptors. J Neurophysiol.

94:4544-4553.
Szikra T and Krizaj D (2005) The role of voltage-operated Ca channels, endoplasmic reticulum and mitochondria in compartmentalization of Ca homeostasis in the photoreceptor inner segment. Proc. IOVS Vol. 45, Ft. Lauderdale, FL
Thoreson WB, Rabl K, Townes-Anderson E, Heidelberger R (2004) A highly Ca^{2+}-sensitive pool of vesicles contributes to linearity at the rod photoreceptor ribbon synapse. Neuron. 42:595-605.
Townes-Anderson E, MacLeish PR, Raviola E (1985) Rod cells dissociated from mature salamander retina: ultrastructure and uptake of horseradish peroxidase. J Cell Biol 100:175-188.
Tucker T, Fettiplace R (1995) Confocal imaging of calcium microdomains and calcium extrusion in turtle hair cells. Neuron 15:1323-1335.
Verweij J, Kamermans M, Spekreijse H (1996) Horizontal cells feed back to cones by shifting the cone calcium-current activation range. Vision Res 36:3943-3953.
Vessey JP, Stratis AK, Daniels BA, Da Silva N, Jonz MG, Lalonde MR, Baldridge WH, Barnes S (2005) Proton-mediated feedback inhibition of presynaptic calcium channels at the cone photoreceptor synapse. J Neurosci. 25:4108-4117
Winkler BS (1983) Relative inhibitory effects of ATP depletion, ouabain and calcium on retinal photoreceptors. Exp Eye Res 36:581-594.
Zhou Z, Neher E (1993) Mobile and immobile calcium buffers in bovine adrenal chromaffin cells. J Physiol. 469:245-273.
Zufall F, Leinders-Zufall T, Greer CA (2000) Amplification of odor-induced $Ca^{(2+)}$ transients by store-operated $Ca^{(2+)}$ release and its role in olfactory signal transduction. J Neurophysiol. 83:501-512.

Figure Legends:

Figure 1. (A) Schematized generic photoreceptor. In addition to the outer segment which hosts the phototransduction apparatus, the cell consists of three distinct subregions: the ellipsoid contains most of cell's mitochondria; the cell body is filled by the nucleus and ER cisternae and the synaptic terminal is packed with vesicles and a few cisternae of

smooth ER. (B) Dissociated salamander rod and (C) Salamander cone photoreceptor. Abbreviations: PMCA = plasma membrane Ca ATP-ase; SERCA = sarcoplasmic-endoplasmic reticulum Ca^{2+} ATPase; VGCC = voltage-gated channel; ER = endoplasmic reticulum; Ca^{2+} sequestration and release from the mitochondria occurs via Ca^{2+} uniporter channels and Na^{+}/Ca^{2+} transporters, respectively. Scale bars = 5 μm.

Figure 2. Spatiotemporal $[Ca^{2+}]$i differences in IS subregions in response to depolarization. (A) Rod photoreceptor superfused for 20 sec with 30 mM KCl. Fast kinetics, high amplitude and spatially localized depolarization-evoked $[Ca^{2+}]_i$ are observed in the synaptic terminal. The free $[Ca^{2+}]$i signal amplitude is sharply delimited between the terminal, the cell body, the subellipsoid and the ellipsoid regions. The gain of the terminal region in the image was increased relative to the rest of the cell (as denoted by the yellow line) to enhance weak fura-2 fluorescence within the terminal (B) Detail of $[Ca^{2+}]_i$ elevation in a rod terminal triggered by transient depolarization. High-amplitude hotspot $[Ca^{2+}]$ increases are observed during depolarization (arrowheads).

Figure 3. Summary of the high K^{+} evoked $[Ca^{2+}]_i$ elevations in regions of rod and cone photoreceptors downstream from the OS.

Figure 4. The amplitude of depolarization-evoked $[Ca^{2+}]$i increases in cell bodies of axotomized rods is not significantly different from $[Ca^{2+}]$i increases in intact cells. (A) Transmission image of an intact rod with a synaptic terminal. (B) Transmission image following terminal axotomy by a sharp microelectrode. (C) Summary data for baseline $[Ca^{2+}]$i (2 mM KCl) and depolarization-evoked (30 mM KCl) $[Ca^{2+}]$i levels in cell bodies from intact cells possessing synaptic terminals. (D) Summary data for baseline $[Ca^{2+}]$i (2 mM KCl) and depolarization-evoked (30 mM KCl) $[Ca^{2+}]$i levels in cell bodies of cells with severed terminals.

Figure 5. A. Isolated ellipsoid and a putative spiking neuron incubated for 30 sec in 0.01% toluidine blue. The ellipsoid was not stained by the vital dye. Scale bar = 10 μm. B. i-iii. A large single cone and an isolated ellipsoid double labeled with TMRM (100

nM) and MitoTracker Green (200 nM). Both indicator dyes selectively label the ellipsoid region in intact cells and following ellipsoid dissociation from the cell body. Ci-iii. Antimycin (10 μM) reduces the TMRM, but not MitoTracker Green, signal within the ellipsoid. D. Confocal linescan of TMRM-positive region in isolated cone ellipsoid during exposure to the mitochondrial uncoupler antimycin. Antimycin depolarizes the membrane potential across the inner mitochondrial membrane, seen as a decrease in ellipsoid TMRM fluorescence.

Figure 6. L-type Ca^{2+} channels are expressed in cone ellipsoids (A) Intact cone transiently depolarized by puffs of 90 mM KCl. 2 μM nifedipine reversibly reduced depolarization-evoked $[Ca^{2+}]$i transients in the cell body (solid trace) and the ellipsoid (dotted trace). (B) Isolated cone ellipsoids express indigenous voltage-operated Ca^{2+} channels. 60 mM KCl- induced $[Ca^{2+}]_i$ elevation is strongly suppressed by 2 μM nifedipine.

Figure 7. Kinetics of depolarization-evoked $[Ca^{2+}]$i responses in photoreceptor compartments. (A) Simultaneous recording of $[Ca^{2+}]_i$ elevations in the cone cell body (black), ellipsoid (blue) and an isolated cone ellipsoid (red trace). The position of the regions of interest is indicated in the inset at the upper right panel. The fastest and largest $[Ca^{2+}]$i change occurred in the cell body while a moderate elevation was recorded in the ellipsoid. The amplitude and kinetics of the high K^+ -evoked $[Ca^{2+}]_i$ response were further reduced in the isolated ellipsoid. (B) High resolution detail from A emphasizes the differences in kinetics between cell regions by enlarging the first segment of the high K^+-induced $[Ca^{2+}]_i$ response. (C & E) Kinetics of $[Ca^{2+}]_i$ rise times and (D & F) $[Ca^{2+}]_i$ decays in cone cell bodies, ellipsoids and isolated ellipsoids in response to 30 mM and 60 mM KCl stimulation, respectively.

Figure 8. Compartmentalized expression of voltage-operated Ca^{2+} channels and PMCAs in salamander photoreceptors. (A) DIC image of the vertical sections of the outer retina of the tiger salamander and (B) Fluorescent micrographs of the retina stained with antibodies raised against α_1 subunits of L type Ca^{2+} channels (pan α_1). Puncta in the

OPL, corresponding to photoreceptor terminals, are strongly stained (arrows), with moderate labeling of the cell body (arrowheads). The putative processes of Müller glia are labeled throughout. (C) DIC image of the salamander outer retina; (D) Fluorescent micrographs of the retina labeled for the PMCA transporter isoform 1 (PMCA1). Synaptic terminals are strongly immunoreactive (arrows), whereas a weaker PMCA1 signal is observed in the cell body (arrowheads). Scale bars = 10 μm.

Figure 1

Click here to download high resolution image

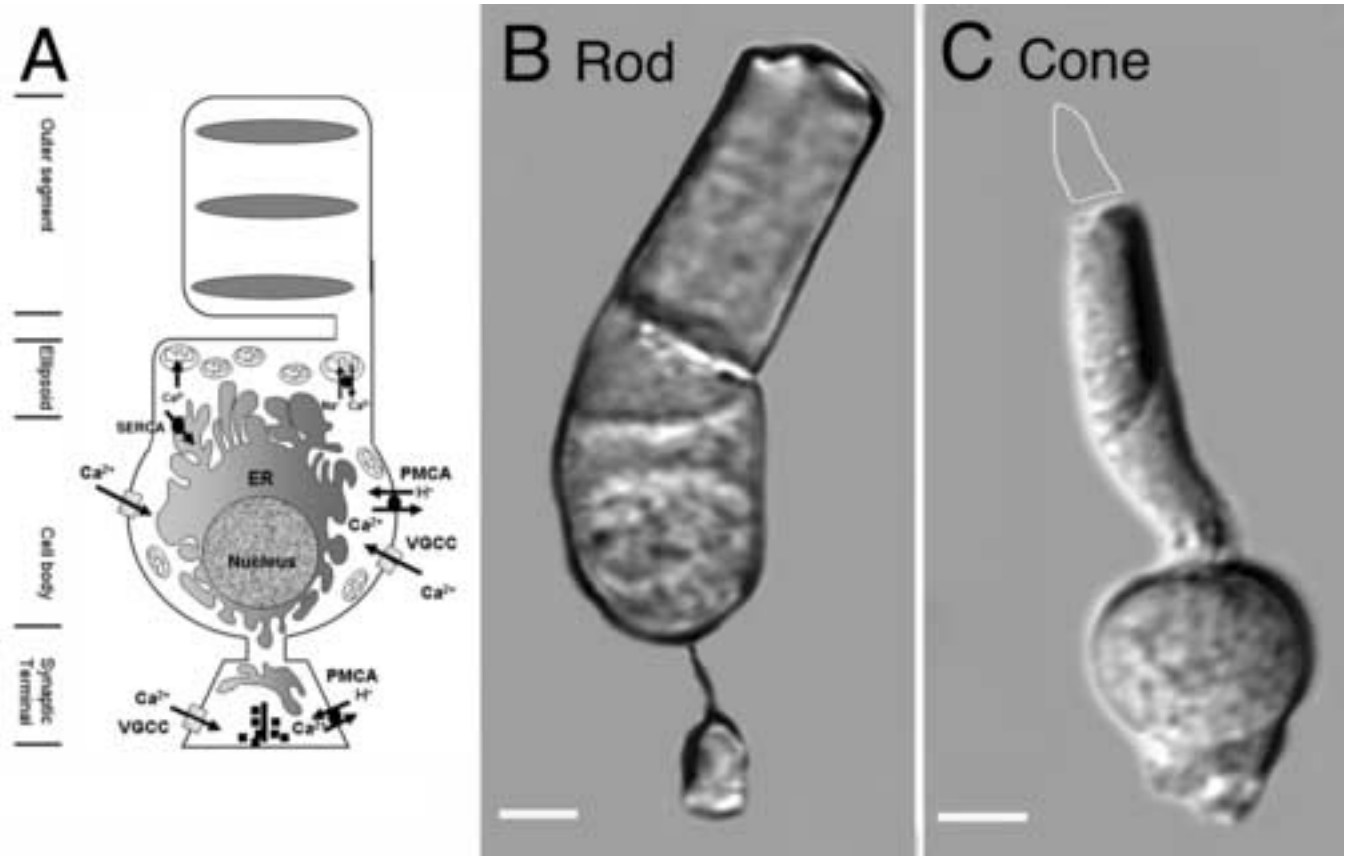

Figure 2

Click here to download high resolution image

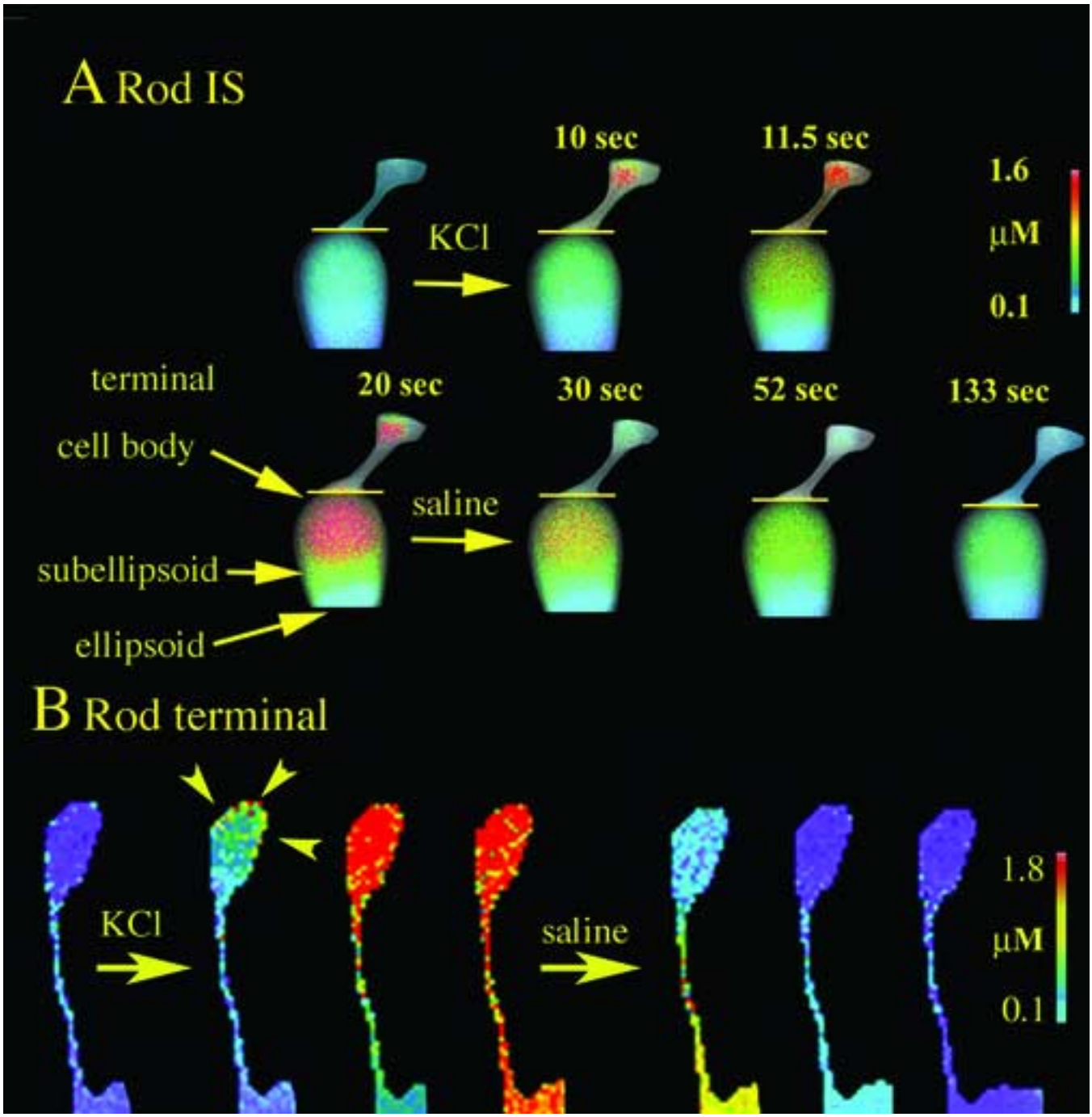

Figure 3

Click here to download high resolution image

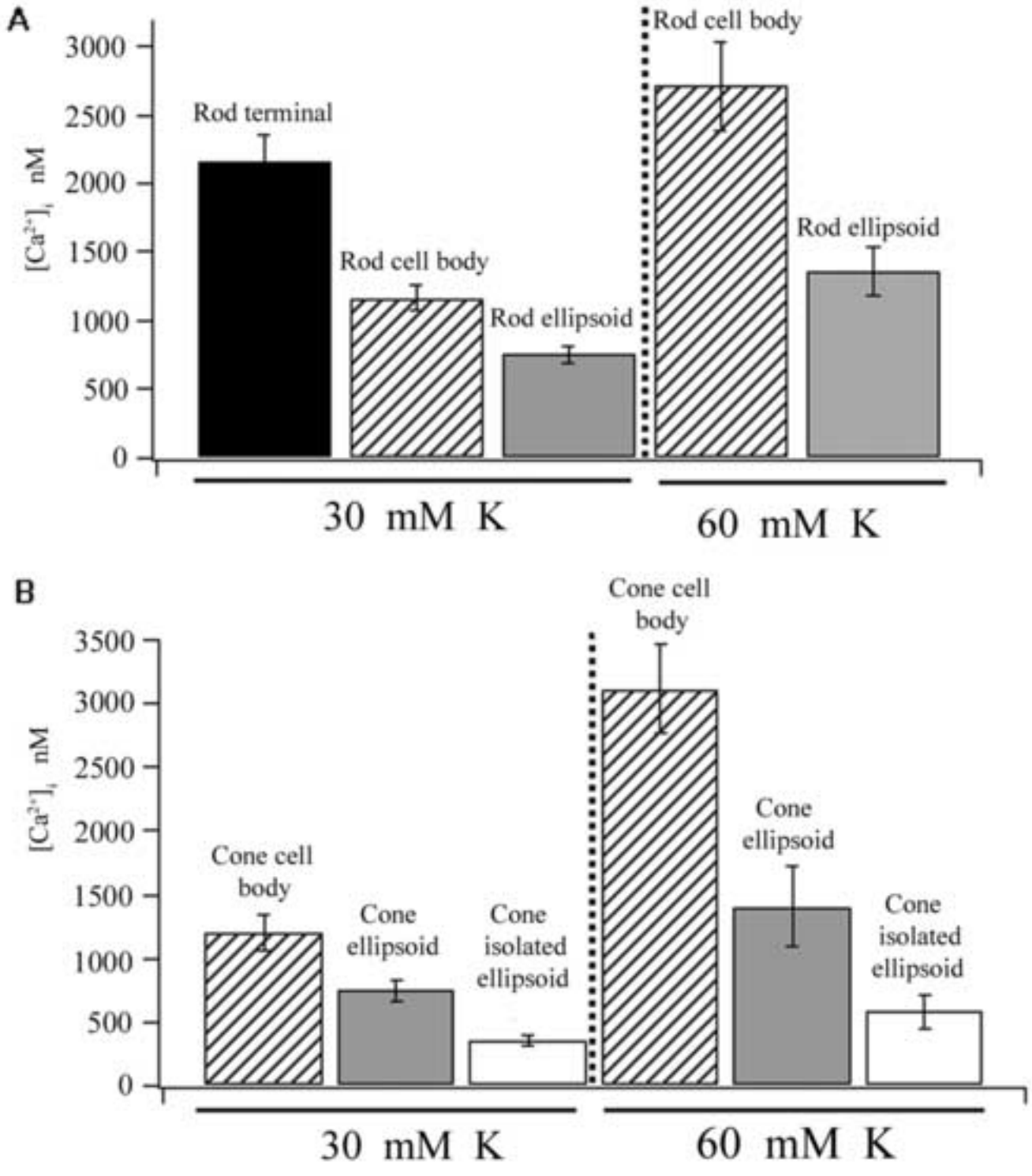

Figure 4

Click here to download high resolution image

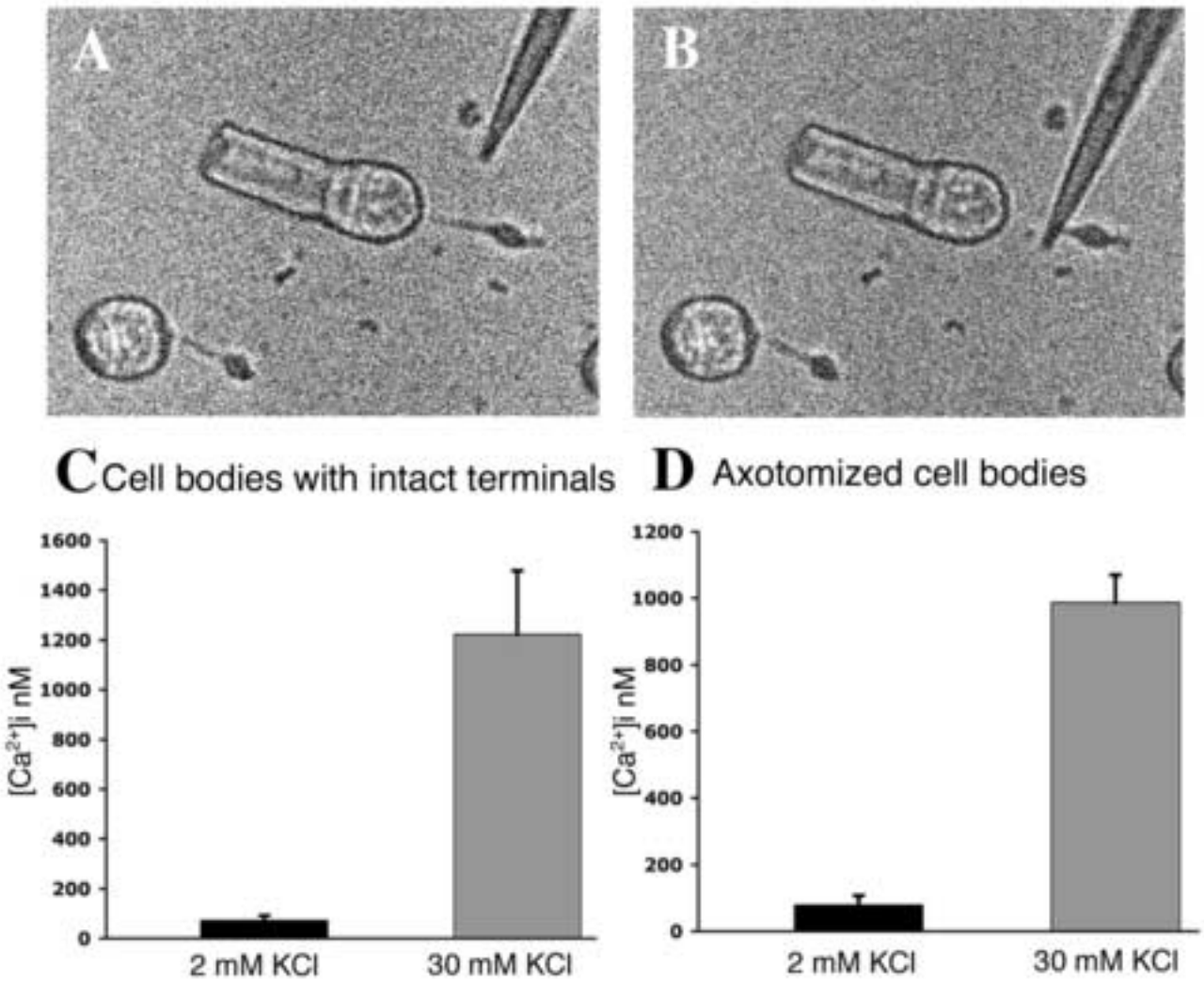

Figure 5

Click here to download high resolution image

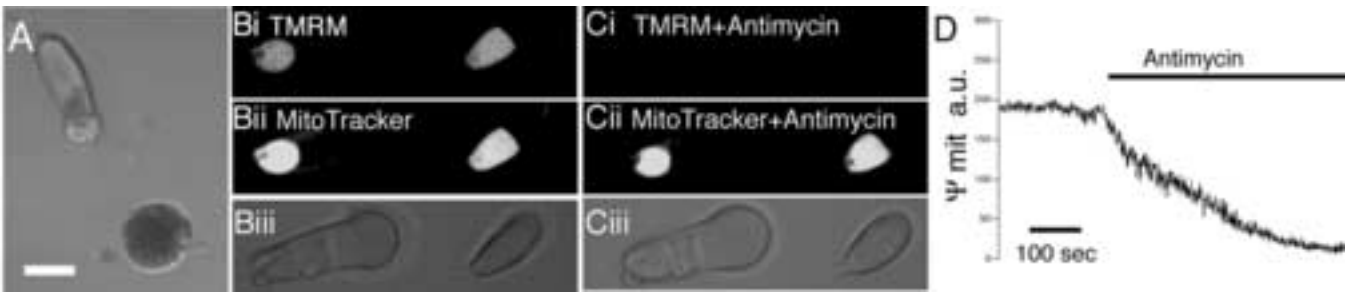

Figure 6

Click here to download high resolution image

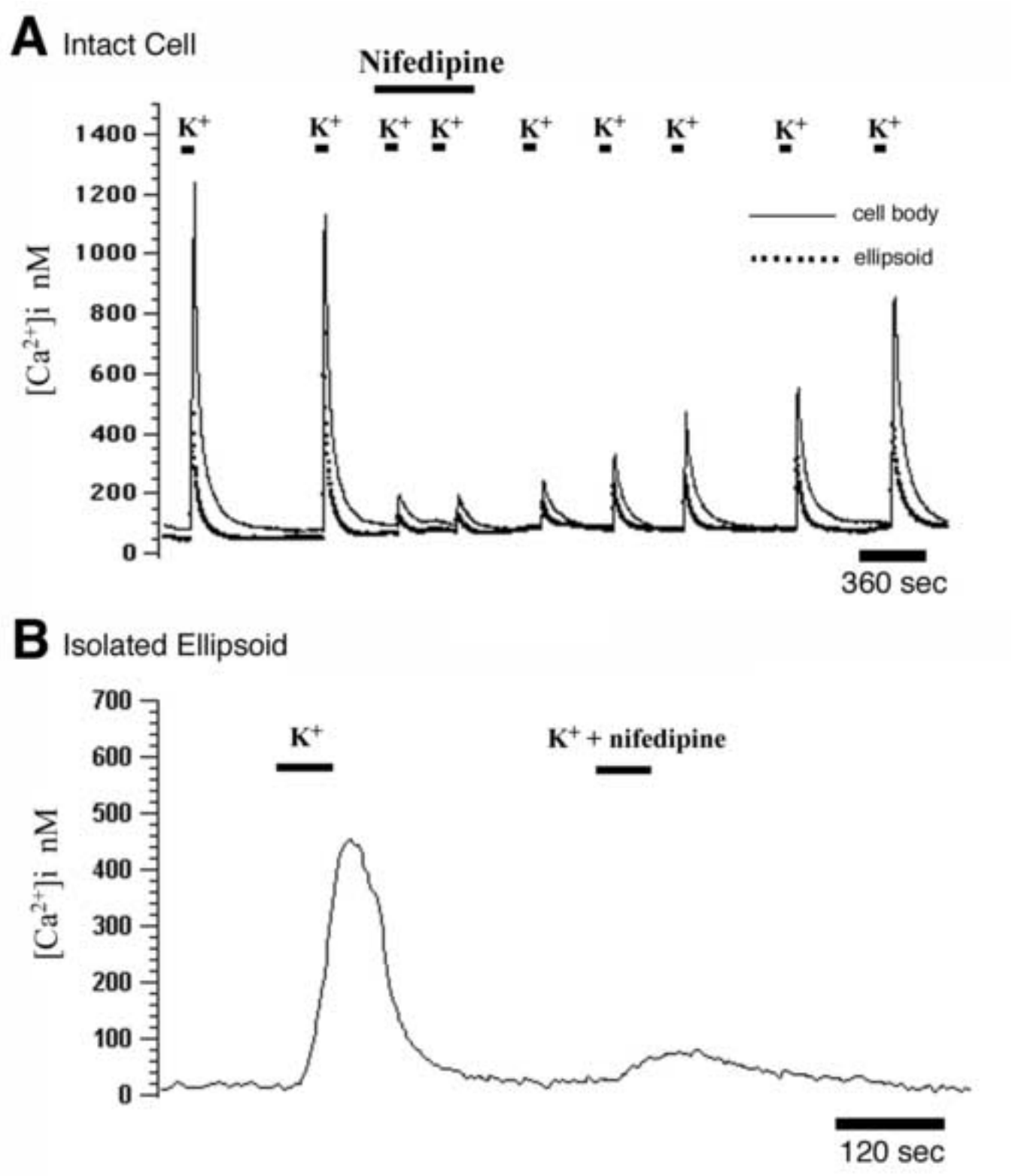

Figure 7

Click here to download high resolution image

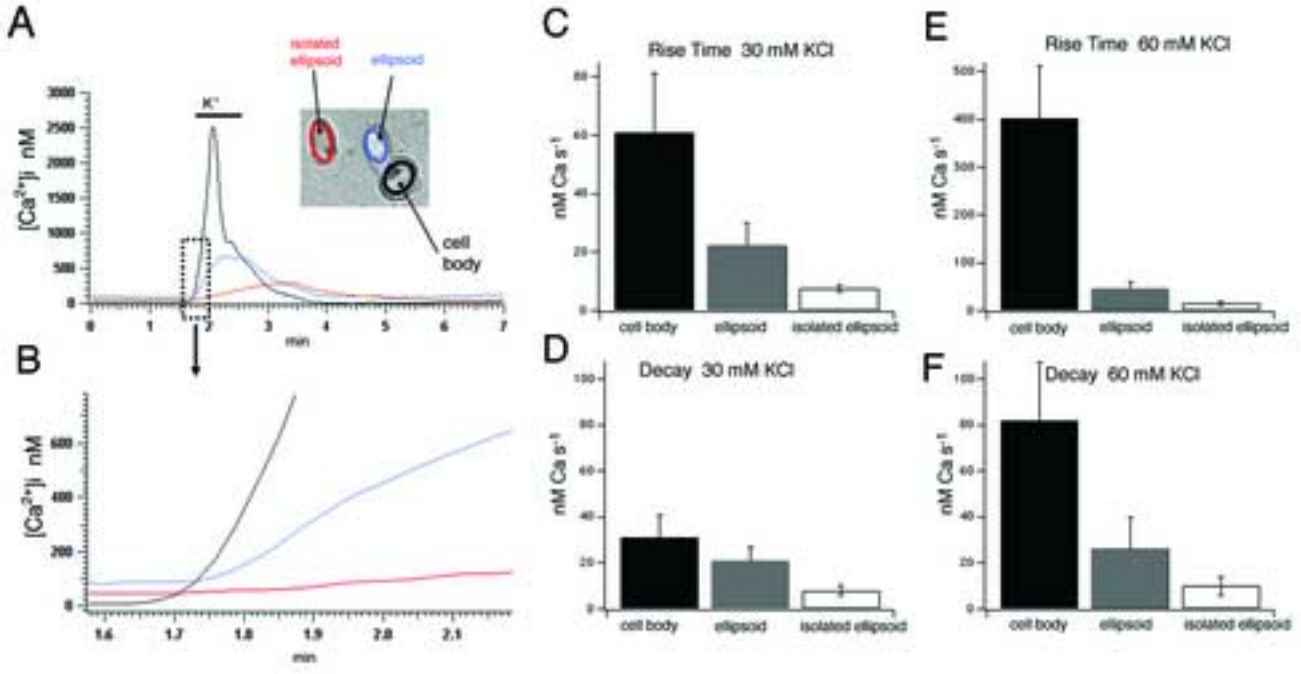

Figure 8

Click here to download high resolution image